

# What is the diatomic molecule with the largest dipole moment?

Ahmed Elhalawani,<sup>1</sup> Ruiren Shi,<sup>1</sup> Mateo Londoño,<sup>1</sup> Michał Tomza,<sup>2</sup> and Jesús Pérez-Ríos<sup>1,\*</sup>

<sup>1</sup>*Department of Physics and Astronomy, Stony Brook University, 11794 Stony Brook, NY, USA*

<sup>2</sup>*Faculty of Physics, University of Warsaw, Pasteura 5, 02-093 Warsaw, Poland*

(Dated: July 15, 2025)

We present a machine learning model for predicting the electric dipole moment of diatomic molecules using only the atomic properties of the constituent atoms. Our model can screen the entire periodic table and identify the molecules with the largest dipole moment for applications in cold molecular sciences, or find the molecule with the largest dipole moment that contains a given atom. Similarly, our model identifies useful trends that explain the dipole moment of molecules, improving our intuition in chemical physics. Finally, we condense our model into an analytical expression to predict the dipole moment in terms of atomic properties.

The electric dipole moment is an intrinsic property or fingerprint of molecules; hence, every molecule has a different one. In cold molecular sciences, the search for diatomic molecules with large dipole moments is one of the most active research areas due to its prospective applications in dipolar quantum gases, the development of quantum gates based on polar molecules [1–6], implementation of new Hamiltonians and the study of many-body physics [7–13], among others. Similarly, the search for new physics with molecules can benefit from molecules with larger dipole moments, especially those containing radioactive atoms like Fr-Y for hadronic charge-parity violation searches [14, 15] and Ra-Y for measuring the electric dipole moment of the electron as a consequence of charge-parity-time-reveral symmetry violation [16, 17].

The dipole moment of molecules is either experimentally determined via spectroscopic techniques or calculated via ab initio quantum chemistry techniques. However, neither of these routes is a plausible approach for determining the dipole moment of the possible 6903 polar diatomic molecules. In principle, one can resort to the chemical intuition to find molecules with the largest difference in the electronegativity within the atoms and, with it, the largest dipole moments due to a larger ionic character [18–21]. However, it has recently been found that X-Ag molecules, where X is an alkali-metal atom, exhibit huge dipole moments, which is unexpected based on the predicted minor ionic character these molecules should show since the two atoms have similar electronegativities [14, 22]. On the basis of these results, it certainly is not a trivial task to find out which diatomic molecules can show a large dipole moment, even though this is supposed to be one of the simplest exercises in chemical physics.

In this Letter, we employ a machine learning approach to predict the dipole moment of diatomic molecules based on atomic properties. As a result, it is possible to screen the whole set of polar diatomic molecules and find which molecules have the largest dipole moment, or to find the molecule containing a given atom type that shows the largest dipole moment. In the same vein, our machine learning models help us identify unforeseen pat-

terns in the dipole moments of molecules based on groups and periods, which are tested against high-level ab initio electronic structure methods and confirmed. Therefore, a machine can teach us more about the nature of the dipole moment and its interconnection with essential atomic properties than anticipated. In line with these findings, we use symbolic regression to identify a simple, data-driven relationship that predicts the dipole moment with an accuracy of better than one Debye.

As introduced by Pauling [18], the polarity of a bond is a direct consequence of atoms having different specificities to attract electrons, known as electronegativity  $\chi$ . Therefore, it is possible to describe the partial ionic character in terms of the electronegativity, and surprisingly enough there is no unique way to do so. Pauling proposed

$$\text{IC}_P = 100 \left( 1 - e^{-\frac{|\chi_1 - \chi_2|^2}{4}} \right), \quad (1)$$

where  $\chi_i$  is the electronegativity of the  $i$ -th atom in the molecule. Alternatively, Hannay and Smyth [20] proposed

$$\text{IC}_{HS} = 16|\chi_1 - \chi_2| + 3.5|\chi_1 - \chi_2|^2. \quad (2)$$

Both of these definitions, Eqs. (1) and (2) lead to very different partial ionic characters, even though both of them were empirically derived [23].

Additionally, as shown beautifully in the seminal work of Coulson [24], the dipole moment has contributions beyond the bond polarity, such as the homopolar dipole moment, in relation to the size of the atom, or the anisotropy of the atomic orbitals. Therefore, the relationship between the dipole moment and the partial ionic character may not be as straightforward as thought, and certainly may depend on properties beyond the electronegativity. However, the idea that electronegativity difference of atoms within a molecule yields a large ionic character, and with it a large dipole moment, is that spread in modern chemistry that even advanced large language models fail to predict the dipole moment of molecules. For instance ChatGPT will give us “Francium fluoride (FrF) is

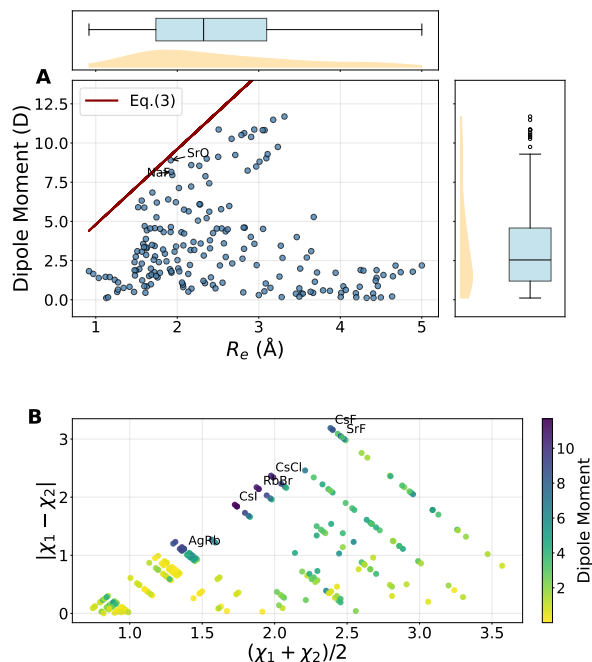


FIG. 1. The dipole moment of diatomic molecules dataset containing experimental and accurate theoretical data. Panel A shows the dipole moment (in Debye) versus the equilibrium distance (in Angstrom), as well as the maximal predicted values from Eq. (3) (for  $q = e$ ) as a dotted line and the 2 molecules with values closest to this prediction. Additionally it shows box plots for the dipole moment and equilibrium distance. The box plot shows the minimum, the maximum, the sample median, and the first and third quartiles of a given distribution. Panel B displays the Arkel-Ketelaar’s triangle of the dataset, as characteristic in inorganic chemistry to characterize metallic (left corner), ionic (top corner), or covalent compounds (right corner).

predicted to have the largest dipole moment, due to the extreme electronegativity difference (F being the highest, Fr the lowest) and the longer bond length from francium’s large atomic radius.”, when we ask about the diatomic molecule with the largest dipole moment. Hence, a more complete understanding on the nature of the dipole moment is required and its relationship with the essential atomic properties of the atoms.

The dipole moment, as it is thought in elementary chemistry courses, is defined as

$$d = qR_e, \quad (3)$$

where  $q$  is the effective separated charge and  $R_e$  denotes the equilibrium bond length of the molecule. As introduced by Pauling, the dipole moment is related to the polarity of molecular bonds, describing the partial ionic character of the bond, given by

$$\text{IC}_d = 100 \frac{d}{eR_e}, \quad (4)$$

where  $e$  is the electron charge, and the result is given in

%.

Here, we pursue a machine learning approach. To learn the dipole moment of diatomic molecules we compile a dataset comprising of 273 molecules. Of these, 140 have experimentally measured dipole moments [25–41], while the remaining 133 have theoretically calculated dipole moments [22, 42–44] using the gold standard in quantum chemistry: Coupled clusters with singles, doubles and perturbatively triple excitations CCSD(T), which is adequate for the determination of most of the diatomics [45]. First, we noticed that the relationship between the dipole moment and the equilibrium distances, using Eq.(3) yields a rather disperse value of  $q$ , as shown in panel A of Fig. 1 and certainly it deviates from the extreme case of  $q = e$ , except NaF and SrO. Therefore, the relationship between the dipole moment and the equilibrium distance is not linear at all for some molecules. To explore the variety of bonding and chemical behavior within this set, we employ the Van Arkel-Ketelaar Triangle [46, 47], as customary in inorganic chemistry to identify the nature of chemical compounds, as shown in panel B of Fig. 1. Molecules closer to the tip of the triangle are those with a larger ionic character (ionic bond), the ones in the right corner show a covalent bond and the ones in the left corner are van der Waals molecules [48]. The data set shows a relatively uniform distribution across these three bonding types, with a slight skew toward van der Waals-type bonding. Interestingly, we noticed that some of the molecules far from the tip of the triangle show a large dipole moment even though its expected ionic character is not large, contradicting the general chemical intuition and classification in chemistry. In particular, the molecules CsI (11.69 Debye), RbBr (10.86 Debye), and CsCl (10.387 Debye) have much larger dipole moments compared to the ionic bond molecules such as CsF (7.88 Debye), SrF (3.47 Debye). What is more remarkable is that there are molecules with a low difference in electronegativity that have comparable dipole moments to ionic bond molecules, such as AgRb (9.03 Debye) and AgCl (5.62 Debye).

We employed Gaussian Process Regression (GPR) as one of our primary predictive model due to its inherent advantages in low-data settings [49]. GPR provides not only point predictions but also uncertainty estimates, which are valuable when applying the model to extrapolate. Additionally, we compare our GPR models against baseline models including Support Vector Regression (SVR), random forest, and Gradient Boosting Regression (GBR), using a consistent validation scheme to ensure a fair comparison. To validate our models, we adopted a Monte Carlo Cross-Validation (MCCV) scheme [50], modified to prevent data leakage from duplicated entries. In each iteration, we randomly split the dataset into 90% training and 10% testing. This split was done based on the Molecule’s name (both the forward and backward versions have the same name in our dataset),

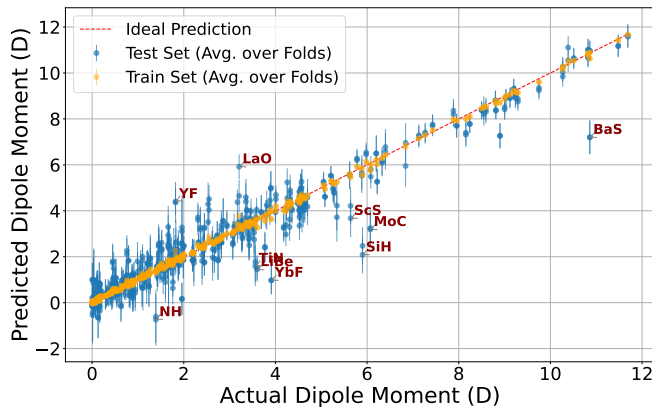


FIG. 2. Prediction of the dipole moment of diatomics. Predicted dipole moment versus the real dipole moment. The error bars represent the associated uncertainty for each prediction, and the dashed red line represents the perfect prediction. The color scheme indicates whether a point belongs to the training set (orange) or the testing set (blue). The labeled points are outliers with  $|\text{Predicted} - \text{Actual}| > 1.5$  Debye.

ensuring that both the original and swapped entries for any given molecule were confined to the same split. This approach prevents information about a molecule in the training set from benefiting predictions in the test set. For all these models, we utilize a modified ionic character provided by Eq. (2)  $\sqrt{IC_{HS}}$  and the difference in ionization potentials (IP)  $\Delta_{IP}^{1/4}$  where  $\Delta_{IP} = |IP_A - IP_B|$  and also the reciprocal product of the ionization potentials  $\frac{1}{IP_A IP_B}$  and the sum of the electron affinities (EA) ( $EA_A + EA_B$ ) for both atoms as numerical features. Additionally, we include the group and period of the atoms within the molecule as categorical features.

ML method	RMSE	MAE
Gaussian Process Regression	0.67	0.45
Gradient Boosting	1.00	0.70
Random Forest	1.05	0.70
Support Vector Regression	1.07	0.77

TABLE I. Comparison of regression methods based on RMSE and MAE (in Debye).

We ran 1000 iterations within the MCCV procedure and computed the average Root Mean Square Error (RMSE) and Mean Absolute Error (MAE) across all runs. The model’s performance, as measured by the MAE and RMSE, is presented in Table I. Therefore, the model only depends on the atomic properties of the atoms. GPR outperforms the other models, with an RMSE of 0.67 Debye, followed by Gradient Boosting Regression. Therefore, from now on, we will focus on the GPR model, and its results are shown in Fig. 2. The

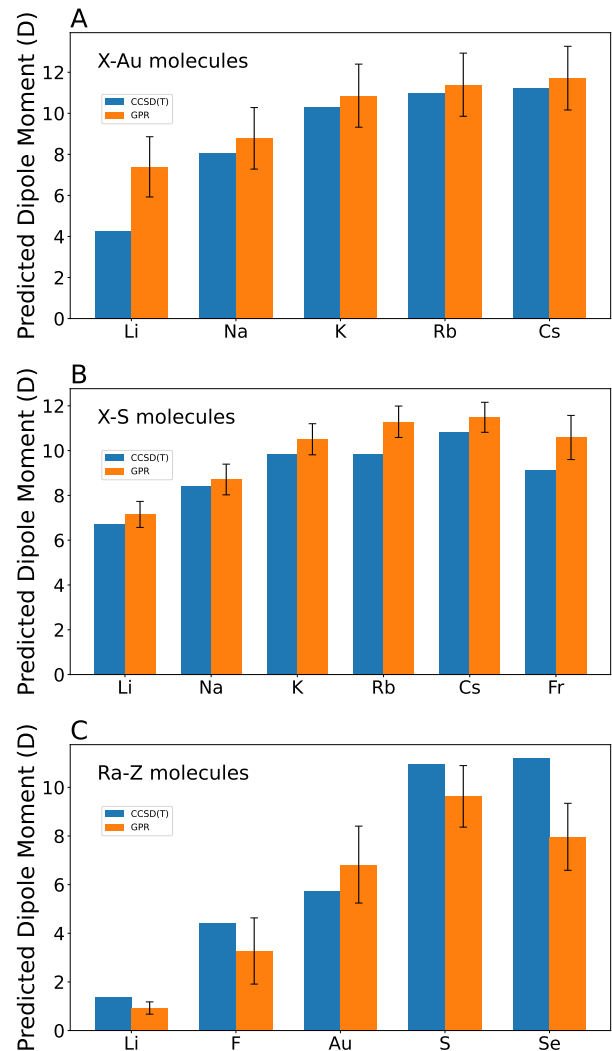


FIG. 3. Testing the machine learning model predictions on 4851 molecules. Panels A and B show the predicted dipole moments for X-Au and X-S molecules ( $X = \text{Alkali-metal}$ ) against CCSD(T), respectively. The machine learning model has never seen these molecules. Lastly Panel C shows Theoretical Dipole Moment for radium-containing Molecules (Ordered by CCSD(T) Smallest to Largest) versus GPR predictions. Across all 3 the trends of CCSD(T) are captured in the GPR predictions.

model presents a few outliers like BaS, MoC, and some van der Waals molecules like LiNa, NaCs, and LiCs, also outliers even when molecular properties are included; possibly related to an anomalous natural bond orbital atomic charge versus the Mulliken charge for each of these molecules [51].

Fueled by the accuracy of the model, we search for the diatomic with the largest dipole moment. Since our model requires the ionic character and, with it, the electronegativities of the atoms, we screen 4851 molecules, as only 99 elements have reliable electronegativities within

the Pauling scale. The results of our model are shown in Fig. 3, in which some unseen molecules by the model are contrasted against CCSD(T) calculations. First, we notice that the model is surprisingly accurate in predicting the dipole moment of unseen molecules in comparison with CCSD(T) calculations, even when some molecules are in the extrapolation regime, i.e., molecules unseen by the model, where machine learning techniques are supposed to lose accuracy. This confirms the robustness of our machine learning model. More importantly, the machine correctly captures the trend for X-Au and X-S molecules, where X is an alkali atom. In other words, the machine is capable of revealing the underlying correlations between the dipole moment and the atomic properties of the atoms forming the molecule.

Recently, it has been demonstrated that alkali-Ag molecules exhibit a significant dipole moment, despite the small electronegativity difference between Ag and alkali atoms. This result is very puzzling. However, as we show in panel A of Fig. 3, alkali-Au molecules show the same trend. Indeed, the dipole moment of alkali-Au molecules is larger than that of alkali-Ag molecules—another example of molecules with a relatively small electronegativity difference showing a large dipole moment. Why is that? The reason is that the group 11 atoms are transition metals with a hole on the valence shell, so they can be seen as the *halogens* of the transition metals. As any halogen, the largest dipole is when those are in contact with alkali atoms, hence explaining why Cu-, Ag-, and alkali-Au have a large dipole moment. Furthermore, alkali-Au molecules show a larger dipole moment than alkali-Ag molecules because Au is larger than Ag, inducing a larger homopolar dipole moment. Following that trend, alkali-Rg may show even larger dipole moments from any of the group 11 elements combined with alkali atoms, although relativistic contributions may affect the dipole moment and ending up comparable to I-alkali molecules. On the other hand, in panel B of Fig. 3, we notice that alkali-S molecules show a pretty significant dipole moment, which should not come a surprise since the alkali-O molecules show a decent dipole moment, keeping in mind that S shows a larger homopolar dipole moment than O. Similarly, if one visualizes S as a p-shell atom with two holes, it should be preferable for them to find a partner with two valence electrons, and those are alkaline-earth atoms. Indeed, S-alkaline-earth molecules show a very large dipole moment.

Another possibility that offer our model is to find the molecule with the largest dipole moment containing a given atom. To test this capability, we predict the radium-containing molecules with the largest dipole moment, and the results against CCSD(T) calculations are shown in panel C of Fig. 3. Again, the GPR model is unexpectedly well in predicting the dipole moment, although RaSe seems a little bit hard for the model. More importantly is that thanks to this exploration, we can

Molecule	CCSD(T)	GPR Prediction	Experimental
CsI	11.73	$11.52 \pm 0.49$	11.69
CsAt	11.72	$10.42 \pm 0.94$	N/A
FrAt	11.64	$9.71 \pm 1.12$	N/A
FrI	11.63	$10.92 \pm 0.85$	N/A
RbI	11.41	$11.15 \pm 0.46$	11.48
CsAu	11.25	$11.82 \pm 0.67$	N/A
RbAu	10.97	$11.76 \pm 0.86$	N/A
CsS	10.82	$11.49 \pm 0.93$	N/A
KAu	10.30	$11.1 \pm 0.85$	N/A
FrAu	9.93	$11.53 \pm 0.98$	N/A

TABLE II. Top 10 molecules with high predicted dipole moments (GPR) and available reference values.

confirm that RaS or RaSe appear as good candidates for the study of radium-containing molecules in the cold regime, and their laser cooling possibilities will be the object of future work.

After the exhaustive screening, we identify the top 10 molecules with the largest dipole moment, and the results are shown in Table II in comparison with CCSD(T) calculations and experimental data, when available. The GPR results are pretty good in comparison with CCSD(T) calculations. The molecule with the largest dipole moment will be the combination between the heavy halogens with alkali atoms X-I or X-At, followed by alkali-Au molecules, which can be seen as the combination of the heaviest halogen transition metal atom and alkali.

To complement our machine learning models, we also applied symbolic regression via PySR [52] to find an analytical formula for the dipole moment of a molecule, AB, in terms of atomic properties

$$d = |\Delta_{IP}^{1/4} + \left( (EA_A + EA_B) \cdot \left( \sqrt{IC_{HS}} \cdot \left( \frac{24.43}{IP_A IP_B} - 0.14 \right) \right) \right)|. \quad (5)$$

The symbolic model achieved an RMSE of 1.26 Debye on the original test data, and when used on the same set of 4851 theoretical molecules, it produced an RMSE of 0.92 Debye, capturing many of the same trends as the machine learning model with reduced precision. The symbolic model offers interpretability and analytic insight that is not as visible when using GPR alone. In other words, we found the most reliable expression for the dipole moment of diatomics.

In summary, we have demonstrated through machine learning that the general idea that the difference in electronegativity determines the polarity of the molecular bond is not the whole picture, as it can lead to erroneous interpretations of the bond in diatomic molecules and fails to predict the dipole moment of diatomics. Thanks to machine learning, we are able to uncover unexpected correlations between the dipole moment and atomic prop-

erties of the constituent atoms that help us better understand the structure of the periodic table and the nature of the dipole moment. In other words, a machine can teach us some basic chemistry. In a more practical sense, and answering the question of the title of this Letter, thanks to a fast screening of diatomic molecules via machine learning techniques, we conclude that the molecules with the largest dipole moment are heavy halogens combined with heavy alkali atoms and Au-alkali molecules, all of them showing dipole  $\gtrsim 11$  Debye. Furthermore, we provide an analytical expression for the dipole moment of diatomics based on symbolic regression, which is the most accurate expression to date for predicting the dipole moments of any diatomic molecule. Finally, it is worth emphasizing that our machine learning model can predict the dipole moment of molecules containing a specific atom, thereby opening a new avenue for identifying the optimal molecule for testing physics beyond the standard model.

The authors acknowledge the support of the support of the United States Air Force Office of Scientific Research [grant number FA9550-23-1-0202]. M.T. acknowledges the National Science Centre Poland (grant no. 2021/43/B/ST4/03326) for financial support.

## SUPPLEMENTAL INFORMATION

### Machine Learning Methods

In Gaussian Process Regression (GPR), the three most important factors that determine a model’s success are data procurement, feature selection, and the choice of kernel. In this section, we provide a brief overview of how and why we chose to address each of these components in the way that we did.

**Data Procurement:** Our dataset consists of diatomic molecules, represented by the atomic properties of each constituent atom (e.g., electron affinity, mass, polarizability). To eliminate directional bias—i.e., the model learning to favor “atom 1” over “atom 2”—we applied a symmetrization strategy by duplicating each molecule with the atomic indices swapped. This ensures that each molecular pair appears twice in the dataset in reversed order, removing dependence on atom labeling and promoting better generalization.

**Feature Selection:** Feature selection was performed through a combination of physical intuition and statistical techniques. From the outset, we aimed for a model that could predict dipole moments of diatomic molecules using only atomic properties (hence avoiding any molecular properties and making the process of extrapolation cleaner). Initially, we included a slew of different atomic properties (electron affinity, ionization potential, electronegativity, polarizability, atomic masses, atomic radii, etc.). However, this approach proved both computationally expensive and less accurate, as it burdened the model with irrelevant information.

To filter for meaningful features, we first performed Principal Component Analysis (PCA) and observed that removing certain features such as polarizability and atomic radii—increased model performance (i.e., decreased RMSE). We then introduced categorical features (periods and groups), explicitly marking them as categorical rather than numerical to aid GPR in learning. This adjustment further improved model performance. Lastly, since we wanted symmetry to be a priority, we created symmetric modifications of important features (e.g., sum, product, absolute difference), and with the help of symbolic regression, we arrived at the final feature set. These steps resulted in a model that is not only more robust and faster but also capable of extrapolating and identifying qualitative physical trends.

**Kernel Choice:** With the explicit goal of extrapolation in mind, our kernel choice may initially appear counterintuitive: the Radial Basis Function (RBF) kernel. The RBF kernel is defined as:

$$k_{\text{RBF}}(x, x') = a^2 \exp\left(-\frac{\|x - x'\|^2}{2\ell^2}\right),$$

where:

- $x$  and  $x'$  are input data points,
- $a^2$  is the amplitude parameter,
- $\ell$  is the lengthscale hyperparameter,
- $\exp$  is the exponential function, and
- $\|x - x'\|^2$  is the squared Euclidean distance between  $x$  and  $x'$ .

While this kernel is typically used for interpolation problems, excelling at capturing local trends but struggling with extrapolation, it performs well in our case. In particular, the total space of all possible diatomic molecules of interest is limited to

$$\binom{118}{2} = 6903,$$

so problems that may plague RBF kernels (e.g., short lengthscales or poor generalization) are less detrimental here. Additionally, while we have a small dataset we made sure that it was chemically diverse (as seen in the Van-Arkel-Ketelaar triangle) ensuring that the model is aware of different bond types and their associated dipole moments.

We compared the RBF kernel to others designed for better extrapolation (e.g., linear, polynomial, and dot-product kernels) and found that they yielded qualitatively similar results and led to the same physical conclusions. However, the RBF kernel consistently produced the most numerically accurate predictions when benchmarked against high-level quantum chemistry results [e.g., CCSD(T)]. The only modification we made was to include a constant kernel alongside the RBF kernel for improved scaling. In conclusion, in spite of its usual shortcomings for extrapolation RBF remains the best kernel choice for our particular problem because of its relatively small size.

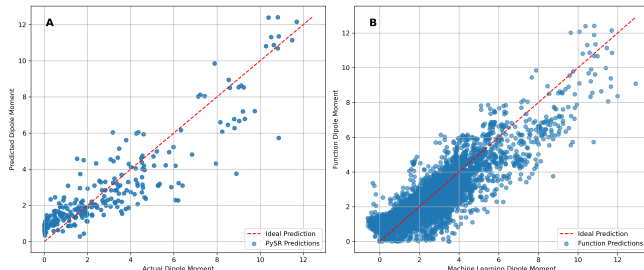


FIG. 4. Figure A displays the PySR analytical model predictions on the y-axis versus the true dipole moment values from the original dataset. Figure B displays the PySR analytical model’s predictions on the y-axis versus the predicted values from the machine learning set of 4,851 molecules.

## Quantum chemistry calculations

### CCSD(T) calculations

The equilibrium bond lengths and dipole moments were calculated at the CCSD(T) level of theory (coupled-cluster with singles, doubles, and perturbative triples) as implemented in the MOLPRO package [53]. For the calculation of the dipole moment, the finite field method was employed.

To ensure a consistent treatment of electron correlation, we employed Dunning’s augmented correlation-consistent basis sets (aug-cc-pVXZ). When core-valence correlation was necessary, we used the polarized weighted core-valence variants (aug-cc-pwCVXZ). For each atom in the system, the appropriate zeta quality was determined through systematic testing to achieve accurate property descriptions.

Additionally, for heavy elements, we used pseudopotentials to describe the core electrons, incorporating scalar relativistic effects accurately. Specifically, for atoms heavier than potassium (K), we applied the Stuttgart energy-consistent effective core potentials (ECPs) in combination with the aug-cc-pVXZ-PP basis sets optimized for these pseudopotentials. For gold, a set of additional  $f$  orbitals with exponents (1.41,0.47,0.15) and  $g$  orbitals with exponents (1.2,0.4) were added along with a contraction re-scaling of 1.5.

The accuracy of the basis sets was assessed by calculating the polarizability and first ionization potential (IP) of the atomic species. The results, along with the specific basis sets used for each atom and the corresponding reference values, are presented in Table IV. Additionally, we computed the equilibrium bond lengths and dipole moments of selected molecules previously reported in the literature, in order to benchmark the performance of the chosen methodology against prior theoretical studies and available experimental data. The results of this molecular benchmarking are summarized in Table III.

### DFT calculations

The equilibrium bond lengths, first order vibrational harmonic frequencies, and dipole moments were calculated with density functional theory (DFT) implemented in the Gaussian 16 program [61].

To achieve high accuracy, we chose the  $\omega$ B97X-D functional, which includes both long-range and short-range exchange correlations, and empirical dispersion corrections, and is reported to generally outperform the commonly used B3LYP functional [62].

For all the atoms reported in this paper, which are mostly S-block and D-block atoms, we used the recommended quadruple zeta valence basis set with two sets of polarization functions (def2-QZVPP), since for DFT

Feature Set	RMSE	MAE
Base	0.8334	0.5903
Base + Polarizability $1/2$ + Mass $1/2$ + Radius $1/2$	0.6984	0.4868
Base + Polarizability $1/2$ + Reduced Mass + Radius $1/2$	0.7075	0.4956
Base + Reduced Mass	0.8750	0.6129
Base - Group	1.1730	0.9418
Base - Period - Group	0.8807	0.5918
Base - Period - Group - Ionic Potential $1/2$	1.2546	0.8431
Base - Period - Group - Electron Affinity $1/2$	1.1820	0.8250
Electronegativity $1/2$ + Ionic Character	1.9249	1.4057
Ionic Character	2.5642	1.7796
Electronegativity $1/2$	1.9066	1.4218
Final	0.6670	0.4500

TABLE III. Comparison of feature sets with RMSE and MAE performance metrics using GPR with the same kernel. **Base** includes: Electronegativities ( $EA_A$ ,  $EA_B$ ), Ionization Potentials ( $IP_A$ ,  $IP_B$ ), Hannay and Smyth Ionic Character ( $IC_{HS}$ ), Periods ( $p_A$ ,  $p_B$ ), and Groups ( $g_A$ ,  $g_B$ ). Final is the final model used in the paper.

Atom	ECP	Basis set	Polarization (au)		IP ( $\text{cm}^{-1}$ )	
			REF. [54]	Calculated	REF. [55]	Calculated
Li	-	aug-cc-pwCVQZ	164.1125	166.106	43488.117	43120.332
Na	-	aug-cc-pwCV5Z	162.7	163.569	41449.430	41391.594
K	-	aug-cc-pwCVQZ	294.3	297.8	35010.621	34930.985
Rb	ECP28MDF	aug-cc-pwCV5Z-PP	319.8	319.6	33691.587	33622.313
Cs	ECP46MDF	aug-cc-pwCV5Z-PP	400.9	397.622	31407.192	31389.254
Fr	ECP78MDF	aug-cc-pwCV5Z-PP	317.8	325.70	37932.239	32431.540
Ca	ECP10MDF	aug-cc-pwCV5Z-PP	160.8	159.28	49307.057	49362.752
Sr	ECP28MDF	aug-cc-pwCV5Z-PP	197.2	198.907	45933.284	45854.457
Ba	ECP46MDF	aug-cc-pwCV5Z-PP	272.0	274.57	42035.842	41895.015
Ra	ECP78MDF	aug-cc-pwCV5Z-PP	246	254.2	42574.342	41507.561
S	-	aug-cc-pwCV5Z	19.4	19.99	83561.097	85876.445
Se	ECP10MDF	aug-cc-pwCV5Z-PP	28.9	24.0d	78659.967	75737.205
F	-	aug-cc-pwCV5Z	3.74	3.40	140527.762	140369.762
I	ECP46MDF	aug-cc-pwCVQZ-PP	32.9	29.80	84292.969	92197.199
At	ECP78MDF	aug-cc-pwCVQZ-PP	42	42.33	75154.711	83075.453
Au	ECP60MDF	aug-cc-pwCV5Z-PP	36	37.21	74410.827	72991.226
Pd	ECP28MDF	aug-cc-pwCV5Z-PP	26.14	26.19	67243.991	67308.517

TABLE IV. Basis sets details along with the values of Polarization and IP for the explored atoms in the CCSD(T) calculations. All the reference values for polarizability and IP were taken from [54] and [55], respectively.

dipole moment calculations, it is close to the DFT basis set limit, and for DFT geometry optimizations, it presents extremely small bases errors [63]. Basis set data for all the atoms are downloaded from Basis Set Exchange [64–66]. The results are presented in Table VI.

#### Machine learning predictions against quantum chemical calculations

In Table VI, we present a comparison between our GPR model prediction of the dipole moment of diatomic



Molecule	$R_{eq}$ (Å)		Dipole (Debye)	
	REF.	Calculated	REF.	Calculated
AuF	1.918 [56]	1.917	4.13[56]	4.33
AuS	2.156 [57]	2.187	2.22 [57]	2.34
SF	1.596 [58]	1.583	0.794 [58]	0.783
SeF	1.714 [59]	1.741	1.520 [59]	1.556
CsI	3.37 [60]	3.340	11.69 [60]	11.733
RbI	3.177 [60]	3.179	11.48 [60]	11.407

TABLE V. Comparison of bond lengths and dipole moments computed using our methodology in MOLPRO with reference values reported in the literature.

versus CCSD(T) and density functional theory (DFT) calculations.

\* [jesus.perezrios@stonybrook.edu](mailto:jesus.perezrios@stonybrook.edu)

- [1] K.-K. Ni, T. Rosenband, and D. D. Grimes, *Chem. Sci.* **9**, 6830 (2018), URL <http://dx.doi.org/10.1039/C8SC02355G>.
- [2] J. Zhu, S. Kais, Q. Wei, D. Herschbach, and B. Friedrich, *The Journal of Chemical Physics* **138**, 024104 (2013), ISSN 0021-9606, [https://pubs.aip.org/aip/jcp/article-pdf/doi/10.1063/1.4774058/14791601/024104\\_1.online.pdf](https://pubs.aip.org/aip/jcp/article-pdf/doi/10.1063/1.4774058/14791601/024104_1.online.pdf), URL <https://doi.org/10.1063/1.4774058>.
- [3] D. DeMille, *Phys. Rev. Lett.* **88**, 067901 (2002), URL <https://link.aps.org/doi/10.1103/PhysRevLett.88.067901>.
- [4] J. L. Bohn, A. M. Rey, and J. Ye, *Science* **357**, 1002 (2017), URL <https://api.semanticscholar.org/CorpusID:206656605>.
- [5] F. Schäfer, T. Fukuhara, S. Sugawa, Y. Takasu, and Y. Takahashi, *Nature Reviews Physics* **2**, 411 (2020), URL <https://doi.org/10.1038/s42254-020-0195-3>.
- [6] J. Pérez-Ríos, *An Introduction to Cold and Ultracold Chemistry* (Springer International Publishing, Cham, Switzerland, 2020), ISBN 3030559351.
- [7] A. Kruckenhauser, L. M. Sieberer, L. De Marco, J.-R. Li, K. Matsuda, W. G. Tobias, G. Valtolina, J. Ye, A. M. Rey, M. A. Baranov, et al., *Phys. Rev. A* **102**, 023320 (2020), URL <https://link.aps.org/doi/10.1103/PhysRevA.102.023320>.
- [8] A. Micheli, G. K. Brennen, and P. Zoller, *Nature Physics* **2**, 341 (2006), URL <https://doi.org/10.1038/nphys287>.
- [9] J. Pérez-Ríos, F. Herrera, and R. V. Krems, *New Journal of Physics* **12**, 103007 (2010), URL <https://doi.org/10.1088/1367-2630/12/10/103007>.
- [10] L. D. Carr, D. DeMille, R. V. Krems, and J. Ye, *New Journal of Physics* **11**, 055049 (2009), URL <https://doi.org/10.1088/1367-2630/11/5/055049>.
- [11] J. A. Blackmore, L. Caldwell, P. D. Gregory, E. M. Bridge, R. Sawant, J. Aldegunde, J. Mur-Petit, D. Jaksch, J. M. Hutson, B. E. Sauer, et al., *Quantum Science and Technology* **4**, 014010 (2018), URL <https://doi.org/10.1088/2058-9565/aaee35>.
- [12] J. A. Blackmore, L. Caldwell, P. D. Gregory, E. M. Bridge, R. Sawant, J. Aldegunde, J. Mur-Petit, D. Jaksch, J. M. Hutson, B. E. Sauer, et al., *Quantum Science and Technology* **4**, 014010 (2018), URL <https://doi.org/10.1088/2058-9565/aaee35>.
- [13] J. Smucker and J. Pérez-Ríos, *Phys. Chem. Chem. Phys.* **26**, 21513 (2024), URL <http://dx.doi.org/10.1039/D4CP01956C>.
- [14] J. Klos, H. Li, E. Tiesinga, and S. Kotochigova, *New Journal of Physics* **24**, 025005 (2022), URL <https://dx.doi.org/10.1088/1367-2630/ac50ea>.
- [15] A. Marc, M. Hubert, and T. Fleig, *Phys. Rev. A* **108**, 062815 (2023), URL <https://link.aps.org/doi/10.1103/PhysRevA.108.062815>.
- [16] R. F. Garcia Ruiz, R. Berger, J. Billowes, C. L. Binnersley, M. L. Bissell, A. A. Breier, A. J. Brinson, K. Chrysalidis, T. E. Cocolios, B. S. Cooper, et al., *Nature* **581**, 396 (2020), URL <https://doi.org/10.1038/s41586-020-2299-4>.
- [17] S. M. Udrescu, A. J. Brinson, R. F. G. Ruiz, K. Gaul, R. Berger, J. Billowes, C. L. Binnersley, M. L. Bissell, A. A. Breier, K. Chrysalidis, et al., *Phys. Rev. Lett.* **127**, 033001 (2021), URL <https://link.aps.org/doi/10.1103/PhysRevLett.127.033001>.
- [18] L. Pauling, *Journal of the American Chemical Society* **53**, 1367 (1931), URL <https://doi.org/10.1021/ja01355a027>.
- [19] L. Pauling, *The nature of the chemical bond and the structure of molecules and crystals : an introduction to modern structural chemistry (3rd ed.)* (Cornell University Press, Ithaca, N.Y., 1986).
- [20] N. B. Hannay and C. P. Smyth, *Journal of the American Chemical Society* **68**, 171 (1946), <https://doi.org/10.1021/ja01206a003>, URL <https://doi.org/10.1021/ja01206a003>.
- [21] M. Klessinger, *Angewandte Chemie International Edition in English* **9**, 500 (1970), <https://onlinelibrary.wiley.com/doi/pdf/10.1002/anie.197005001>, URL <https://onlinelibrary.wiley.com/doi/abs/10.1002/anie.197005001>.
- [22] M. Śmiałkowski and M. Tomza, *Phys. Rev. A* **103**, 022802 (2021), URL <https://link.aps.org/doi/10.1103/PhysRevA.103.022802>.
- [23] Note1, the main difference is in HF since Pauling assumed a 63 % of partial ionic character whereas Hanny and Smyth assumed a 41 %.
- [24] C. A. Coulson, *Valence* (Clarendon Press, Oxford, Oxford, United Kingdom, 1952).
- [25] L.-R. Liu, M. Aguirre, S. R. Kane, B. K. Kendrick, and B. Hemmerling, *Phys. Rev. A* **111**, 062810 (2025), URL <https://link.aps.org/doi/10.1103/hwmm-1mn7>.
- [26] R. Zhang, T. C. Steimle, L. Cheng, and J. F. Stanton, *Molecular Physics* **113**, 2073 (2015), <https://doi.org/10.1080/00268976.2014.996619>, URL <https://doi.org/10.1080/00268976.2014.996619>.
- [27] H. Wang, X. Zhuang, and T. C. Steimle, *The Journal of Chemical Physics* **131**, 114315 (2009), ISSN 0021-9606, [https://pubs.aip.org/aip/jcp/article-pdf/doi/10.1063/1.3226672/15853028/114315\\_1.online.pdf](https://pubs.aip.org/aip/jcp/article-pdf/doi/10.1063/1.3226672/15853028/114315_1.online.pdf), URL <https://doi.org/10.1063/1.3226672>.
- [28] X. Zhuang and T. C. Steimle, *The Journal of Chemical Physics* **140**, 124301 (2014), URL <https://doi.org/10.1063/1.4868551>.



- [29] L. A. Koelemay and L. M. Ziurys, The Astrophysical Journal Letters **958**, L6 (2023), URL <https://doi.org/10.3847/2041-8213/ad0899>.
- [30] T. C. Steimle, J. Chen, J. J. Harrison, and J. M. Brown, The Journal of Chemical Physics **124**, 184307 (2006), URL <https://doi.org/10.1063/1.2194551>.
- [31] F. A. DeLeeuw and A. Dymanus, Journal of Molecular Spectroscopy **48**, 427 (1973).
- [32] A. Le, T. C. Steimle, L. Skripnikov, and A. V. Titov, The Journal of Chemical Physics **138**, 124313 (2013), ISSN 0021-9606, <https://pubs.aip.org/aip/jcp/article-pdf/doi/10.1063/1.4794049/15462617/124313.1.online.pdf>, URL <https://doi.org/10.1063/1.4794049>.
- [33] X. Zhuang, T. C. Steimle, and C. Linton, The Journal of Chemical Physics **133**, 164310 (2010), ISSN 0021-9606, <https://pubs.aip.org/aip/jcp/article-pdf/doi/10.1063/1.3505141/13521406/164310.1.online.pdf>, URL <https://doi.org/10.1063/1.3505141>.
- [34] H. Wang, W. L. Virgo, J. Chen, and T. C. Steimle, The Journal of Chemical Physics **127**, 124302 (2007), ISSN 0021-9606, <https://pubs.aip.org/aip/jcp/article-pdf/doi/10.1063/1.2778427/10925232/124302.1.online.pdf>, URL <https://doi.org/10.1063/1.2778427>.
- [35] D. A. Fletcher, D. Dai, T. C. Steimle, and K. Balasubramanian, The Journal of Chemical Physics **99**, 9324 (1993), ISSN 0021-9606, <https://pubs.aip.org/aip/jcp/article-pdf/99/11/9324/19058597/9324.1.online.pdf>, URL <https://doi.org/10.1063/1.465503>.
- [36] C. Qin, R. Zhang, F. Wang, and T. C. Steimle, The Journal of Chemical Physics **137**, 054309 (2012), ISSN 0021-9606, <https://pubs.aip.org/aip/jcp/article-pdf/doi/10.1063/1.4734596/15452915/054309.1.online.pdf>, URL <https://doi.org/10.1063/1.4734596>.
- [37] T. C. Steimle, K. Y. Jung, and B. Li, The Journal of Chemical Physics **103**, 1767 (1995), ISSN 0021-9606, <https://pubs.aip.org/aip/jcp/article-pdf/103/5/1767/19169676/1767.1.online.pdf>, URL <https://doi.org/10.1063/1.469750>.
- [38] T. C. Steimle and W. L. Virgo, The Journal of Chemical Physics **121**, 12411 (2004), ISSN 0021-9606, <https://pubs.aip.org/aip/jcp/article-pdf/121/24/12411/19158912/12411.1.online.pdf>, URL <https://doi.org/10.1063/1.1822917>.
- [39] J. Gengler, T. Ma, A. G. Adam, and T. C. Steimle, The Journal of Chemical Physics **126**, 134304 (2007), ISSN 0021-9606, <https://pubs.aip.org/aip/jcp/article-pdf/doi/10.1063/1.2711807/15396366/134304.1.online.pdf>, URL <https://doi.org/10.1063/1.2711807>.
- [40] T. C. Steimle, W. L. Virgo, and T. Ma, The Journal of Chemical Physics **124**, 024309 (2006), ISSN 0021-9606, <https://pubs.aip.org/aip/jcp/article-pdf/doi/10.1063/1.2145880/13217248/024309.1.online.pdf>, URL <https://doi.org/10.1063/1.2145880>.
- [41] F. Wang and T. C. Steimle, The Journal of Chemical Physics **134**, 201106 (2011), ISSN 0021-9606, <https://pubs.aip.org/aip/jcp/article-pdf/doi/10.1063/1.3595469/13538519/201106.1.online.pdf>, URL <https://doi.org/10.1063/1.3595469>.
- [42] H. Ladjimi and M. Tomza, Phys. Rev. A **109**, 052814 (2024), URL <https://link.aps.org/doi/10.1103/PhysRevA.109.052814>.
- [43] M. Tomza, Phys. Rev. A **88**, 012519 (2013), URL <https://link.aps.org/doi/10.1103/PhysRevA.88.012519>.
- [44] M. Tomza, New Journal of Physics **23**, 085003 (2021), URL <https://dx.doi.org/10.1088/1367-2630/ac1696>.
- [45] X. Liu, L. McKemmish, and J. Pérez-Ríos, Phys. Chem. Chem. Phys. **25**, 4093 (2023), URL <http://dx.doi.org/10.1039/D2CP05060A>.
- [46] L. C. Allen, J. F. Capitani, G. A. Kolks, and G. D. Sproul, Journal of Molecular Structure **300**, 647 (1993), ISSN 0022-2860, URL <https://www.sciencedirect.com/science/article/pii/002228609387053C>.
- [47] J. A. A. Ketelaar, *Chemical Constitution: An Introduction to the Theory of the Chemical Bond* (Elsevier Publishing Company, Houston, 1953).
- [48] Note2, note that in the original Van Arkel-Ketelaar Triangle, compounds in the left corner are classified as metallic rather than van der Waals.
- [49] C. K. Williams and C. E. Rasmussen, *Gaussian processes for machine learning*, vol. 2 (MIT press Cambridge, MA, 2006).
- [50] X. Liu, G. Meijer, and J. Pérez-Ríos, *On the universality of spectroscopic constants of diatomic molecules* (2020), 2005.07913.
- [51] X. Liu, G. Meijer, and J. Pérez-Ríos, Phys. Chem. Chem. Phys. **22**, 24191 (2020), URL <http://dx.doi.org/10.1039/D0CP03810E>.
- [52] P. Cranmer, *Interpretable Machine Learning for Science with PySR and SymbolicRegression.jl* (2023), arXiv:2305.01582 [astro-ph, physics:physics], URL <http://arxiv.org/abs/2305.01582>.
- [53] H.-J. Werner, P. J. Knowles, R. Lindh, F. R. Manby, M. Schütz, et al., *Molpro, a package of ab initio programs* (2008), see <http://www.molpro.net>.
- [54] P. Schwerdtfeger and J. K. Nagle, Molecular Physics **117**, 1200 (2019), <https://doi.org/10.1080/00268976.2018.1535143>, URL <https://doi.org/10.1080/00268976.2018.1535143>.
- [55] A. Kramida, Yu. Ralchenko, J. Reader, and NIST ASD Team, NIST Atomic Spectra Database (ver. 5.12), [Online]. Available: <https://physics.nist.gov/asd> [2025, July 3]. National Institute of Standards and Technology, Gaithersburg, MD. (2024).
- [56] Y. Lu, R. Tang, X. Fu, H. Liu, and C. Ning, The Journal of Chemical Physics **154**, 074303 (2021), ISSN 0021-9606, <https://pubs.aip.org/aip/jcp/article-pdf/doi/10.1063/5.0038560/15585847/074303.1.online.pdf>, URL <https://doi.org/10.1063/5.0038560>.
- [57] R. Zhang, Y. Yu, T. C. Steimle, and L. Cheng, The Journal of Chemical Physics **146**, 064307 (2017), ISSN 0021-9606, <https://pubs.aip.org/aip/jcp/article-pdf/doi/10.1063/1.4975816/14776955/064307.1.online.pdf>, URL <https://doi.org/10.1063/1.4975816>.
- [58] T. Amano and E. Hirota, Journal of Molecular Spectroscopy **45**, 417 (1973), ISSN 0022-2852, URL <https://www.sciencedirect.com/science/article/pii/0022285273902129>.
- [59] C. Byfleet, A. Carrington, and D. Russell, Molecular Physics **20**, 271 (1971), <https://doi.org/10.1080/00268977100100251>, URL <https://doi.org/10.1080/00268977100100251>.
- [60] J. Story, T. L. and A. J. Hebert, The Journal of Chemical Physics **64**, 855 (1976), ISSN 0021-9606, <https://pubs.aip.org/aip/jcp/article-pdf/64/2/855/18898914/855.1.online.pdf>, URL <https://doi.org/10.1063/1.432235>.

- [61] M. J. Frisch, G. W. Trucks, H. B. Schlegel, G. E. Scuseria, M. A. Robb, J. R. Cheeseman, G. Scalmani, V. Barone, G. A. Petersson, H. Nakatsuji, et al., *Gaussian 16 Revision C.01* (2016), Gaussian Inc. Wallingford CT.
- [62] J.-D. Chai and M. Head-Gordon, *Phys. Chem. Chem. Phys.* **10**, 6615 (2008).
- [63] F. Weigend, F. Furche, and R. Ahlrichs, *The Journal of chemical physics* **119**, 12753 (2003).
- [64] B. P. Pritchard, D. Altarawy, B. Didier, T. D. Gibson, and T. L. Windus, *Journal of chemical information and modeling* **59**, 4814 (2019).
- [65] D. Feller, *Journal of computational chemistry* **17**, 1571 (1996).
- [66] K. L. Schuchardt, B. T. Didier, T. Elsethagen, L. Sun, V. Gurumoorthi, J. Chase, J. Li, and T. L. Windus, *Journal of chemical information and modeling* **47**, 1045 (2007).

Molecule	CCSD(T)	DFT	GPR	GPR Lower Bound	GPR Upper Bound
BaAu	4.3630	5.5464	6.02	5.13	6.92
CaAu	3.6100	2.6427	4.55	3.72	5.38
CsAu	11.2520	10.8127	11.82	10.89	12.74
AuF	4.2090	nan	4.82	4.25	5.39
KAu	10.3050	9.8416	11.10	10.25	11.95
LiAu	4.2450	6.1492	7.56	6.80	8.33
NaAu	8.0510	7.7114	9.68	8.86	10.50
RaAu	5.7260	nan	6.40	5.46	7.34
RbAu	10.9720	10.5441	11.76	10.90	12.62
AuS	2.3200	nan	2.00	1.11	2.89
SrAu	4.1890	3.6073	5.57	4.73	6.40
KPd	7.7110	nan	6.33	5.25	7.41
LiPd	4.5270	nan	4.37	3.40	5.35
RbPd	8.0290	nan	6.18	5.09	7.27
RaF	4.4320	nan	3.19	2.05	4.34
LiRa	1.3960	nan	0.427	0.165	0.756
RaSe	11.1960	nan	7.98	7.08	8.88
BaS	10.8850	11.6329	6.58	5.83	7.34
CaS	10.1480	11.3756	8.24	7.73	8.76
CsS	10.82	10.3621	11.49	10.82	12.20
BaSe	11.1770	12.1959	8.59	7.98	9.20
CaSe	10.0310	11.5003	6.71	6.10	7.35
CsSe	11.0790	10.8586	10.58	9.81	11.34
SeF	1.5560	nan	1.33	0.70	1.96
KSe	10.2350	10.8360	9.86	9.12	10.60
LiSe	6.8400	7.2794	6.26	5.63	6.70
NaSe	8.6190	8.9761	7.95	7.24	8.65
RbSe	10.8310	11.5469	10.71	9.97	11.45
SrSe	10.6540	12.1073	4.59	3.78	5.40
SF	0.7830	nan	1.70	1.08	2.32
KS	9.8680	10.6156	10.51	9.81	11.21
LiS	6.7080	7.2321	7.15	6.57	7.73
NaS	8.4280	8.9388	7.95	7.24	8.65
RbS	9.8240	11.2679	11.29	10.59	11.99
SrS	10.6230	11.8811	4.76	3.92	5.60
FrS	9.14	nan	10.58	9.60	11.57

TABLE VI. CCSD(T) vs DFT vs GPR